SIS Receivers for Submillimeter Wave Astronomy

T. G. Phillips, Thomas H. Büttgenbach and Brian N. Ellison

Division of Physics, Mathematics and Astronomy, California Institute of Technology, Pasadena, CA 91125

We report on the development of broadband heterodyne receiver systems used at the Caltech Submillimeter Telescope (CSO) on Mauna Kea, Hawaii. All our receivers utilize Pb alloy superconductor insulator superconductor (SIS) tunnel junctions for the mixing element. Standard electron beam lithography for the masks and the tri–level photoresist stencil technique are used for the fabrication. Typical gap voltages of 2.4 mV and critical current densities of about 7000 A/cm^2 at 4.2 K are achieved. The junction overlap area is between 0.5 and 1.0 μm^2 yielding $\omega R_N C$ = 1 at about 150 GHz. These devices are fabricated in collaboration with Ronald E. Miller at AT&T Bell Laboratories (Figure 1). Receiver noise temperatures of about 65 K (DSB) at 220 GHz and 150 K (DSB) at 350 GHz are achieved.

Waveguide receivers

Two waveguide receivers are currently operated at the CSO (henceforth referred to as the 230 GHz and 345 GHz receiver). The receivers are designed to operate from 190 to 290 GHz (Ellison and Miller 1987) and 280 GHz to 420 GHz (Ellison et al. 1989). A schematic layout of the receiver system is shown in figure 2. The IF is 500 MHz wide and centered at 1.5 GHz. The three stage IF amplifier (Weinreb et al. 1982) has been modified to have a HEMT in its first stage yielding about 2 K noise temperature.

Both mixers have two noncontacting shorts, i.e. a backshort and an E plane tuner, in full height waveguide (Figures 3,4). The shorts are formed from a series of high and low impedance sections. Their design center frequency is 230 GHz and 345 GHz for the two receivers. Originally the SIS junction was mounted on the waveguide wall with an asymmetric filter structure (RF choke). Again the design center frequency for the RF chokes is 230 GHz and 345 GHz. Scale model measurements, which are discussed in more detail below, showed that the desired position for the junction is in the center of the waveguide. Both mixer blocks are now in that configuration.

The 230 GHz receiver has been tested successfully over its design frequency range (Figure 5). The best sensitivity obtained for this receiver is at 220 GHz with a double sideband (DSB) noise temperature of 65 K. Typical values are about 100 K. The 345 GHz receiver has yet not been tested above 370 GHz due to lack of local oscillator power. Its best performance is at 345 GHz with T_{DSB} = 150K and typical value of about 200 K (Figures 6,7). The performance of both receivers is best close to the design center frequency for the RF choke and the sliding shorts and degrades towards both ends of the band. Thus we conclude that the performance of the receivers far away from the center frequency is limited by the RF choke or the sliding shorts rather than the ability to match power into the junction mount. Figure 8 shows a comparison of the best reported noise temperatures of broadband heterodyne receivers. All numbers were converted to single sideband noise temperatures for purposes of comparison.

The waveguide blocks are mounted in hybrid cryostats using CTI closed cycle refrigerators to cool the IF amplifiers and radiation shields to 12 K and a liquid Helium reservoir to cool the mixer blocks (Ellison 1988, Figure 9). The 4 liter liquid helium reservoir has a hold time of 18 days.

Scale Model and theory for the waveguide receivers

The 230 GHz waveguide receiver in its original configuration showed a region of very high noise temperatures at about 250 GHz. We built a scale model of the mixer block (Figure 10) in order to investigate this resonance and the general performance of the two tuner waveguide structure (Büttgenbach et al. 1990). The two tuners allow access to a wide range of impedances as shown by the shaded area in Figure 11. The

dark circles are backshort circles, i.e. the E plane tuner was fixed and the back short moved. Figure 12 shows the performance over the fundamental waveguide band of the model. The transmission data was obtained by sending power into the waveguide port, where the horn antenna would be located in the full size mixer and taken out with the probes at the junction position. The tuners were optimized for each data point. Comparing Figure 12a with 12b shows that the transmission is highest where the area of accessible impedance values in the Smith chart is largest. Figure 12c demonstrates this by depicting the relative tuning area, i.e. the ratio of accessible tuning area to total area of the Smith chart. The qualitative behavior of the transmission and relative tuning area as a function of frequency is identical. Deducing the efficiency of a mount geometry by comparing the measured embedding impedances with the desired impedance for a device can be misleading. This is well demonstrated at the resonance frequency at 6.4 GHz. Depending on what one assumes for the embedding impedance of the SIS junction one could come to the conclusion that the SIS junction is well matched to the incoming radiation. As apparent from figure 12b this is not the case. The relative tuning area, however, is much more significant. This is due to the fact that a tuner has a zero reflection coefficient for a non propagating mode. The large range of impedance values available when moving the tuners allows good coupling to the propagating mode in the waveguide, which contains the energy of the incoming radiation.

Figure 13 shows the relative tuning area as a function of junction position in the waveguide. The resonance strength decreases significantly when the junction is centered. Numerical simulations (Büttgenbach et al. 1990) of the same waveguide structure showed the same effect. This resonance is due to cross modal coupling to all n=1 modes caused by the junction mount as represented by an obstacle in the waveguide. By centering the gap, i.e. the position where the junction is in the waveguide, the coupling to the n=1 modes can be eliminated and therefore the strength of the resonance reduced. This has been confirmed in the 230 GHz receiver, when the SIS junction was moved into the center of the waveguide. The noise temperature at the resonance frequency (250 GHz) is now only a factor of 1.5 higher than the average value in the vicinity.

According to theory the resonance frequency is inversely proportional to the waveguide height. The effective waveguide height at the mount is somewhat higher than the geometric height due to the dielectric substrate of the junction mount. The decrease of resonance frequency due to the substrate dielectric has been investigated and found to be in excellent agreement with the measured resonance frequency of the 230 GHz receiver.

Fabrication of reduced height waveguide components in the submillimeter region is very difficult, making it advantageous to maintain full height waveguide. However, a slight reduction in waveguide height ($\approx 20\%$) will push the resonance out of the frequency range of interest without increasing machining difficulty significantly.

Figure 14 shows a lumped element equivalent circuit derived from the theory. L_1 and C_1 correspond to the reactance due to the coupling to the n=1 modes. C and L contain the reactances of the coupling to all other modes, the lead inductances, the junction capacitance and the choke reactance. At the resonance frequency, i.e. where L_1 and C_1 resonate, the junction is shorted.

Quasi optical receivers

We are investigating a new technique of coupling the radiation from a telescope into an SIS detector by means of planar antennas instead of waveguide structures. This technique avoids the difficulty of fabricating waveguide structures in the submillimeter band, which become very lossy. Furthermore there is the potential for a receiver operating over several octaves. A major disadvantage is the lack of tuning capability thus requiring SIS junctions with low $\omega R_N C$ products at the operating frequency. We use a planar antenna mounted on a hyperhemispherical lens (Figure 15) as first suggested by Rutledge. Initial receiver tests (Wengler et al. 1985) using bow–tie antennas were promising. A continued investigation (Büttgenbach et al. 1989) using spiral antennas (Figures 16,17) gave noise temperature results that were almost as good as waveguide systems below 400 GHz and considerably better from 400 GHz to 760 GHz. These results were obtained with one single instrument. However, the coupling efficiency of the receiver to the light from the telescope was rather poor ($\approx 30\%$). This is due to the extremely fast beam launched by the spiral antenna and the problems associated with controlling that beam. We are currently investigating the optics for planar antenna structure receivers with the goal of improving the coupling efficiencies.

References

Büttgenbach, T.H., Groesbeck, T.D., and Ellison, B.N., "A Scale Mixer Model for SIS Waveguide Receivers," Int. J. of IR and MM Waves, vol. 11, no. 1, January 1990.

Büttgenbach, T.H., Miller, R.E., Wengler, M.J., Watson, D.M., Phillips, T.G., "A Broad-Band Low-Noise SIS Receiver for Submillimeter Astronomy, IEEE Trans. Microwave Theory Tech., vol. MTT-36, December 1988.

Ellison, B.N., and Miller, R.E., "A Low Noise 230 GHz Receiver," Int. J. of IR and MM Waves, vol. 8, no. 6, June 1987.

Ellison, B.N., Schaffer, P.L., Schaal, W., Vail, D., and Miller, R.E., "A 345 GHz Receiver for Radio Astronomy," Int. J. of IR and MM Waves, vol. 10, no. 8, 1989.

Ellison, B.N., "Hybrid liquid helium cryostat for radio astronomy use", Cryogenics, vol. 28, November 1988.

Weinreb, S., Fenstermacher, D.L., and Harris, R.W., "Ultra-low-noise 1.2 to 1.7 GHz cooled GaAs-Fet amplifiers", IEEE Trans. Microwave Theory Tech., vol. MTT-30, June 1982.

Wengler, M.J., Woody, D.P., Miller, R.E., and Phillips, T.G., "A Low Noise Receiver for Millimeter and Submillimeter Wavelength," Int. J. of IR and MM Waves, vol. 6, pp. 697-706, 1985.

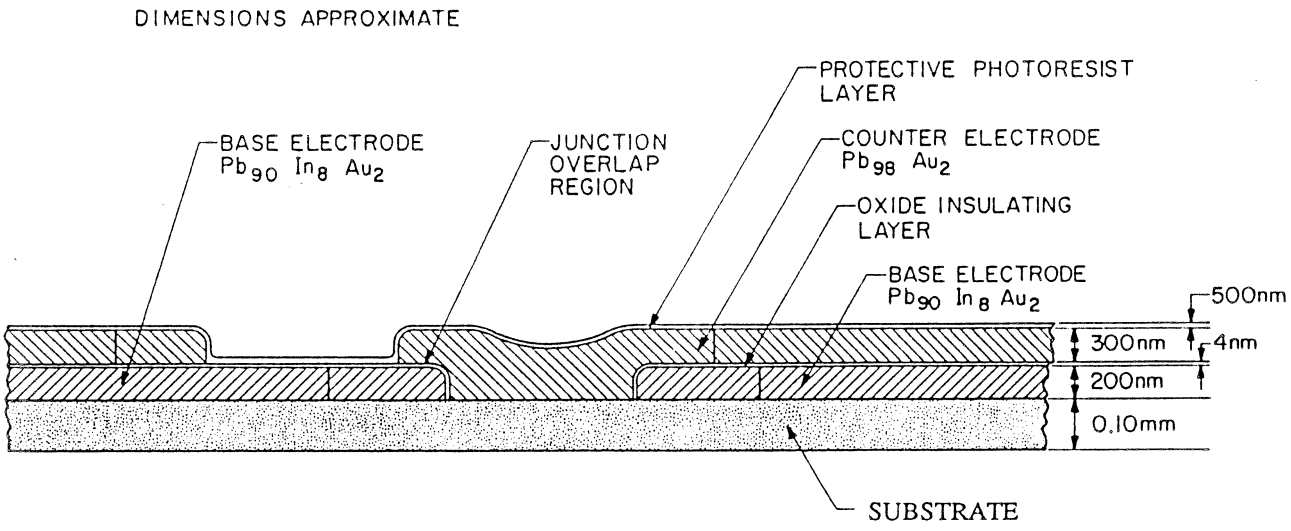
DIMENSIONS APPROXIMATE
PROTECTIVE PHOTORESIST LAYER
BASE ELECTRODE Pb_{90} In_8 Au_2
JUNCTION OVERLAP REGION
COUNTER ELECTRODE Pb_{98} Au_2
OXIDE INSULATING LAYER
BASE ELECTRODE Pb_{90} In_8 Au_2
500nm
300nm
4nm
200nm
0.10mm
SUBSTRATE

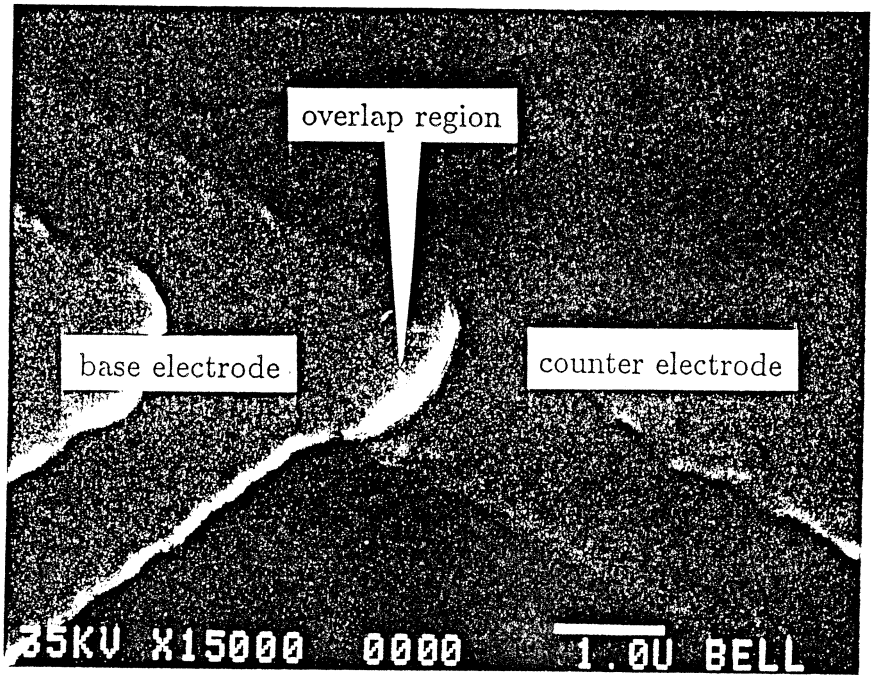
overlap region
base electrode
counter electrode
35KV X15000 0000
1.0U BELL

Figure 1

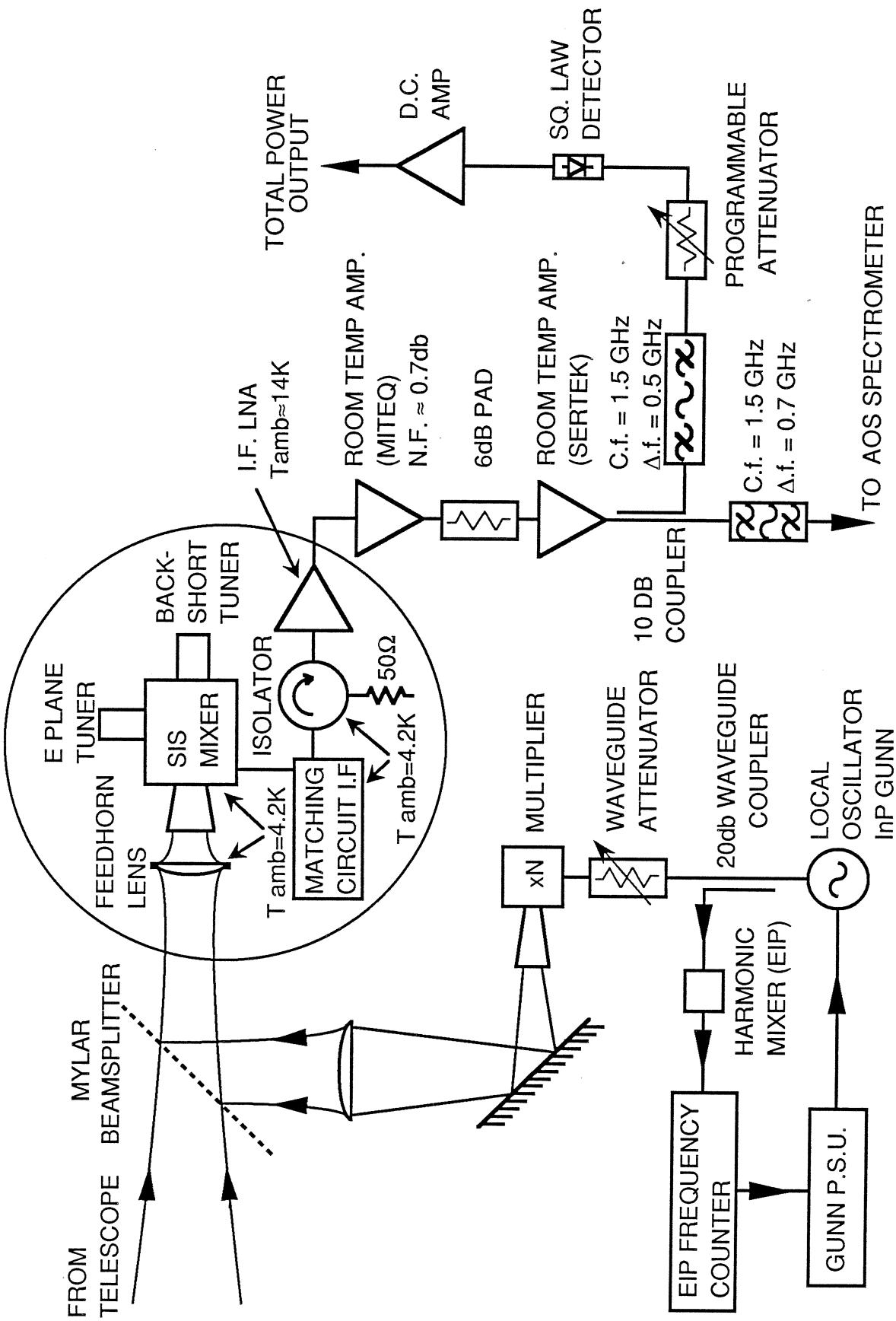
FROM TELESCOPE
MYLAR BEAMSPLITTER
FEEDHORN LENS
E PLANE TUNER
SIS MIXER
BACK-SHORT TUNER
I.F. LNA Tamb≈14K
ISOLATOR
50Ω
T amb=4.2K
MATCHING CIRCUIT I.F
T amb=4.2K
ROOM TEMP AMP. (MITEQ) N.F. ≈ 0.7db
6dB PAD
ROOM TEMP AMP. (SERTEK)
10 DB COUPLER
C.f. = 1.5 GHz
Δ.f. = 0.5 GHz
C.f. = 1.5 GHz
Δ.f. = 0.7 GHz
PROGRAMMABLE ATTENUATOR
SQ. LAW DETECTOR
D.C. AMP
TOTAL POWER OUTPUT
TO AOS SPECTROMETER
MULTIPLIER
xN
WAVEGUIDE ATTENUATOR
20db WAVEGUIDE COUPLER
LOCAL OSCILLATOR InP GUNN
HARMONIC MIXER (EIP)
EIP FREQUENCY COUNTER
GUNN P.S.U.

Figure 2

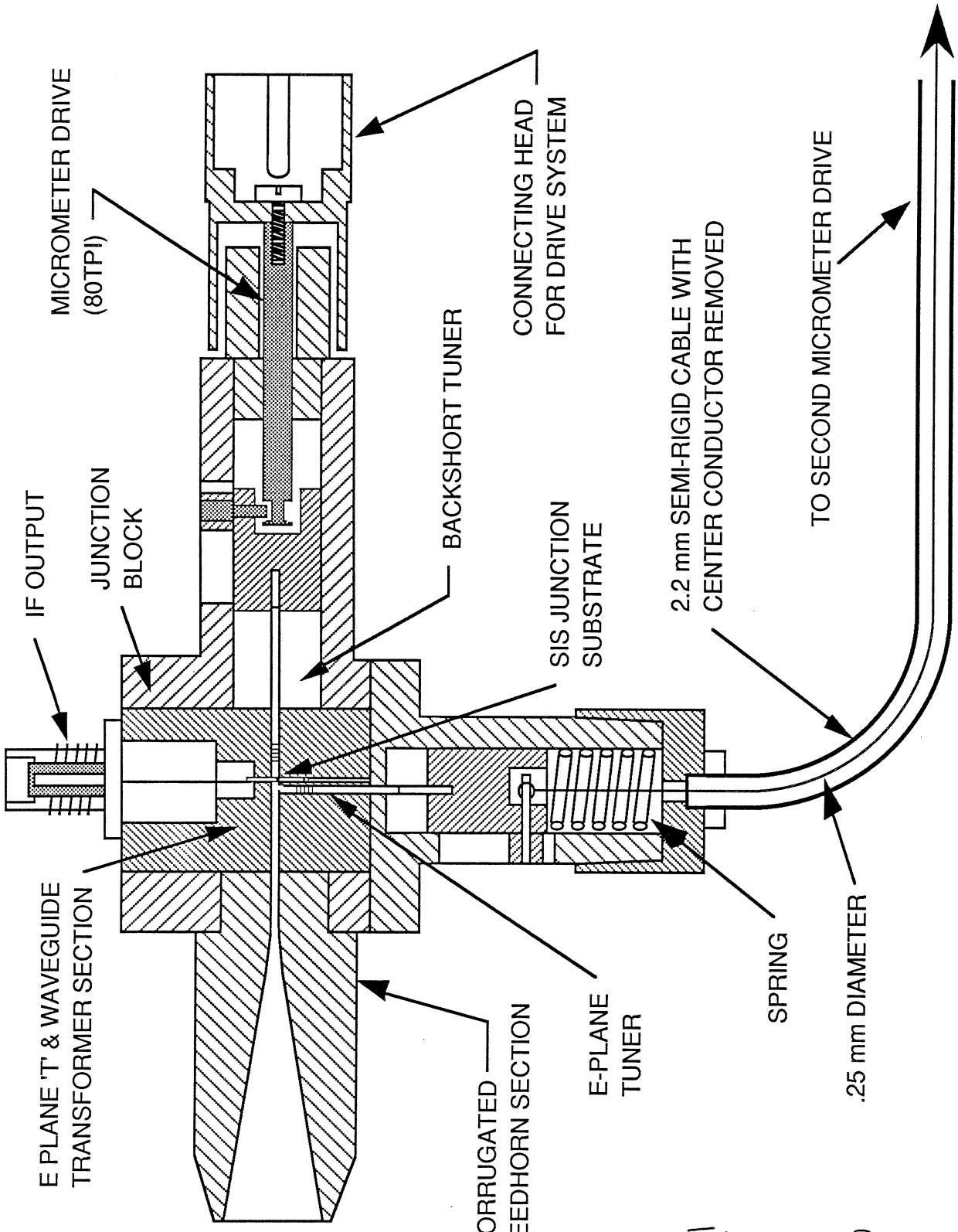
MICROMETER DRIVE
(80TPI)
CONNECTING HEAD
FOR DRIVE SYSTEM
IF OUTPUT
JUNCTION
BLOCK
BACKSHORT TUNER
SIS JUNCTION
SUBSTRATE
2.2 mm SEMI-RIGID CABLE WITH
CENTER CONDUCTOR REMOVED
TO SECOND MICROMETER DRIVE
E PLANE 'T' & WAVEGUIDE
TRANSFORMER SECTION
CORRUGATED
FEEDHORN SECTION
E-PLANE
TUNER
SPRING
.25 mm DIAMETER

Figure 3

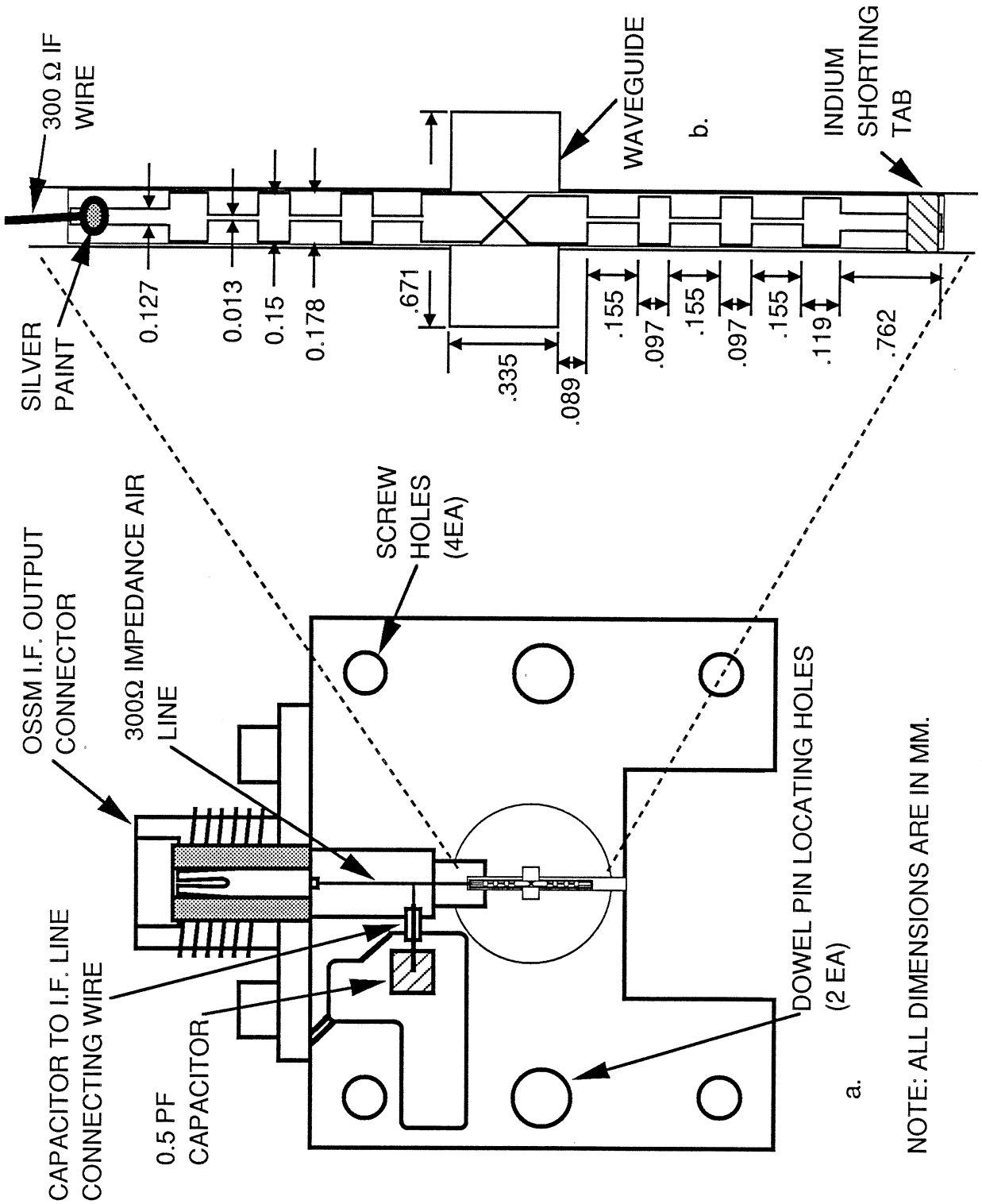
300 Ω IF WIRE
WAVEGUIDE
INDIUM SHORTING TAB
SILVER PAINT
0.127
0.013
0.15
0.178
.671
.335
.089
.155
.097
.155
.097
.155
.119
.762
b.
OSSM I.F. OUTPUT CONNECTOR
300Ω IMPEDANCE AIR LINE
SCREW HOLES (4EA)
CAPACITOR TO I.F. LINE CONNECTING WIRE
0.5 PF CAPACITOR
DOWEL PIN LOCATING HOLES (2 EA)
a.
NOTE: ALL DIMENSIONS ARE IN MM.

Figure 4

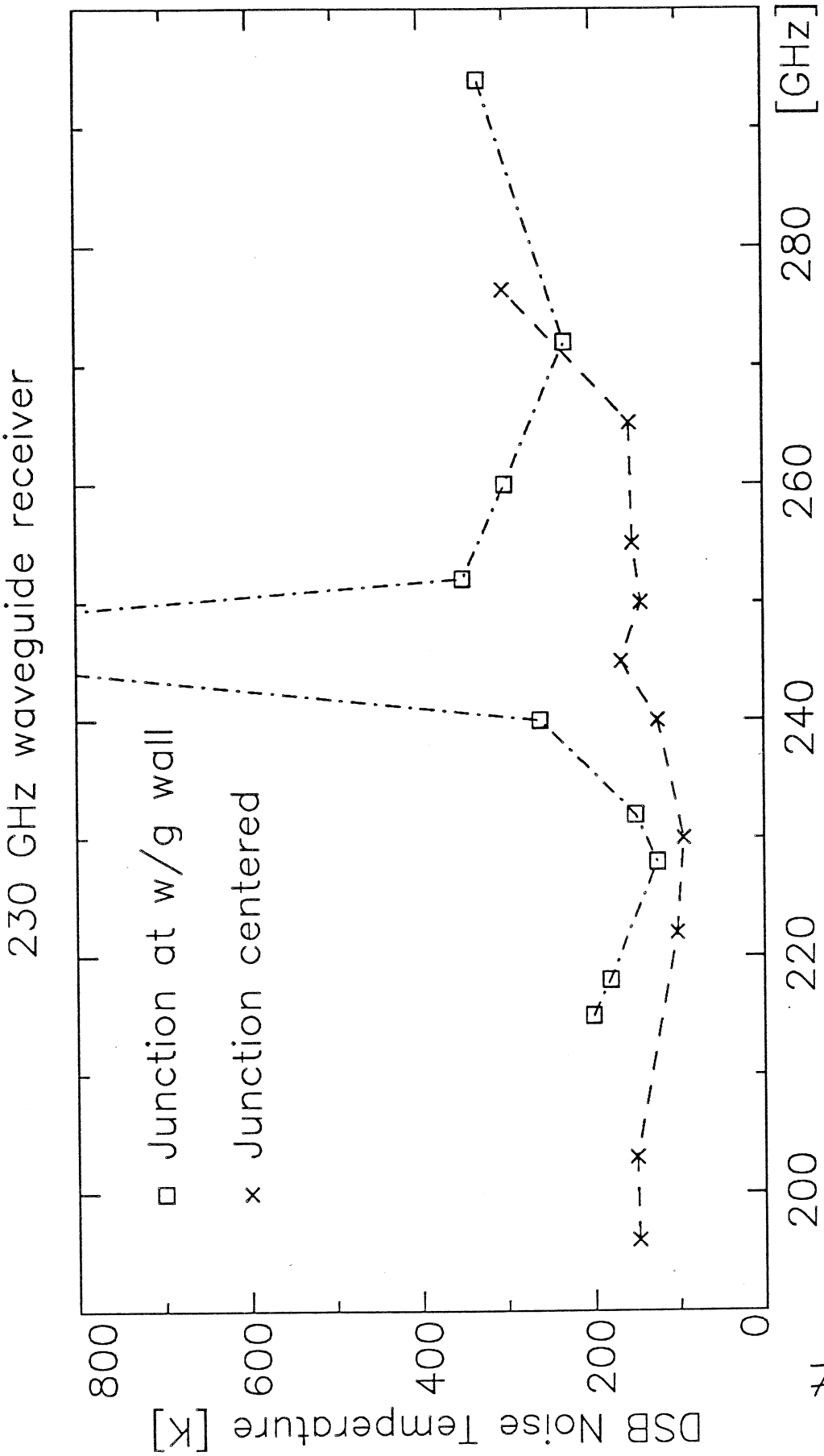
230 GHz waveguide receiver
□ Junction at w/g wall
× Junction centered
DSB Noise Temperature [K]
0
200
400
600
800
Frequency [GHz]
200
220
240
260
280
[GHz]

Figure 5

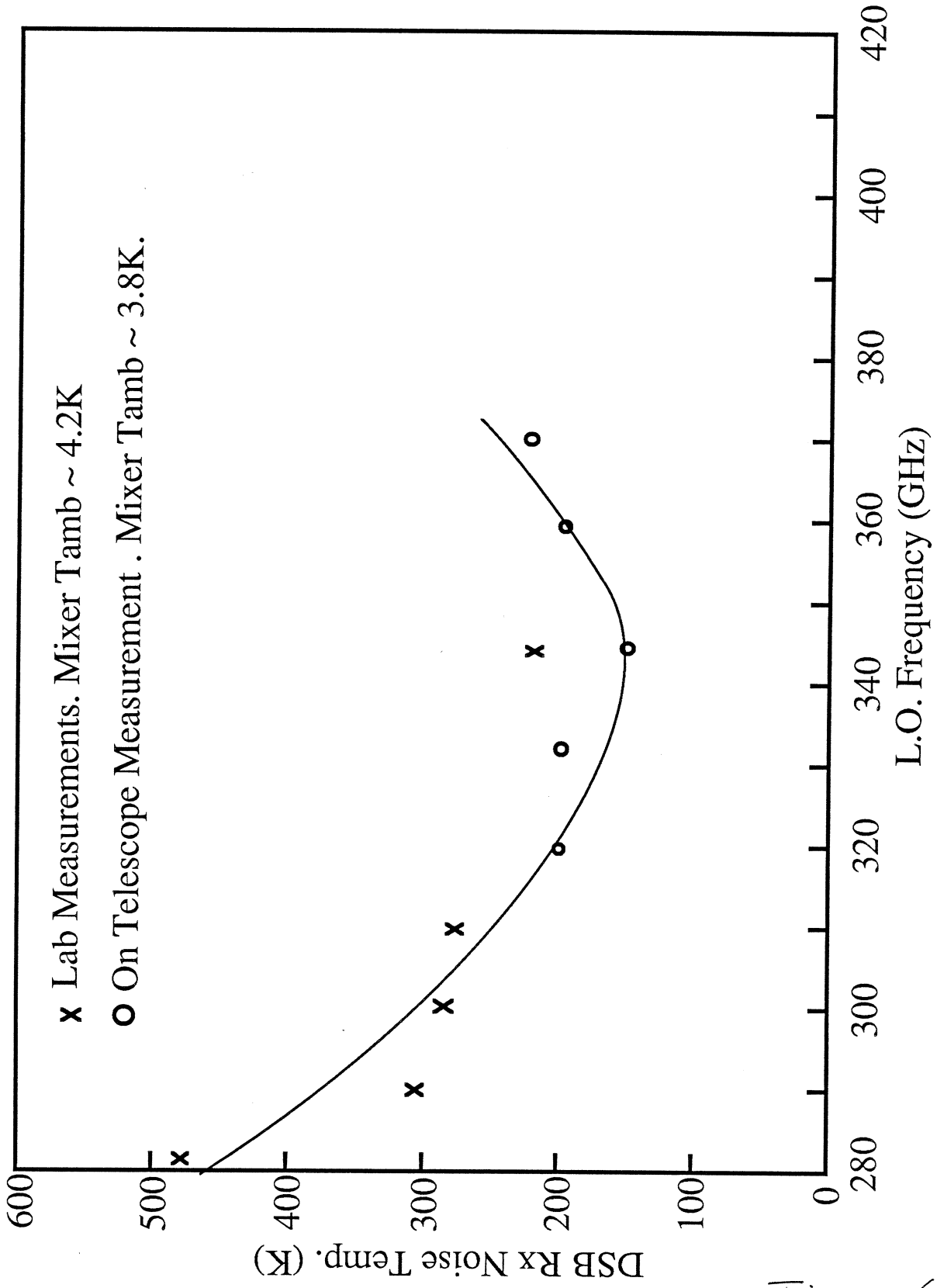
x Lab Measurements. Mixer Tamb ~ 4.2K
o On Telescope Measurement . Mixer Tamb ~ 3.8K.
DSB Rx Noise Temp. (K)
L.O. Frequency (GHz)
600
500
400
300
200
100
0
280
300
320
340
360
380
400
420

Figure 6

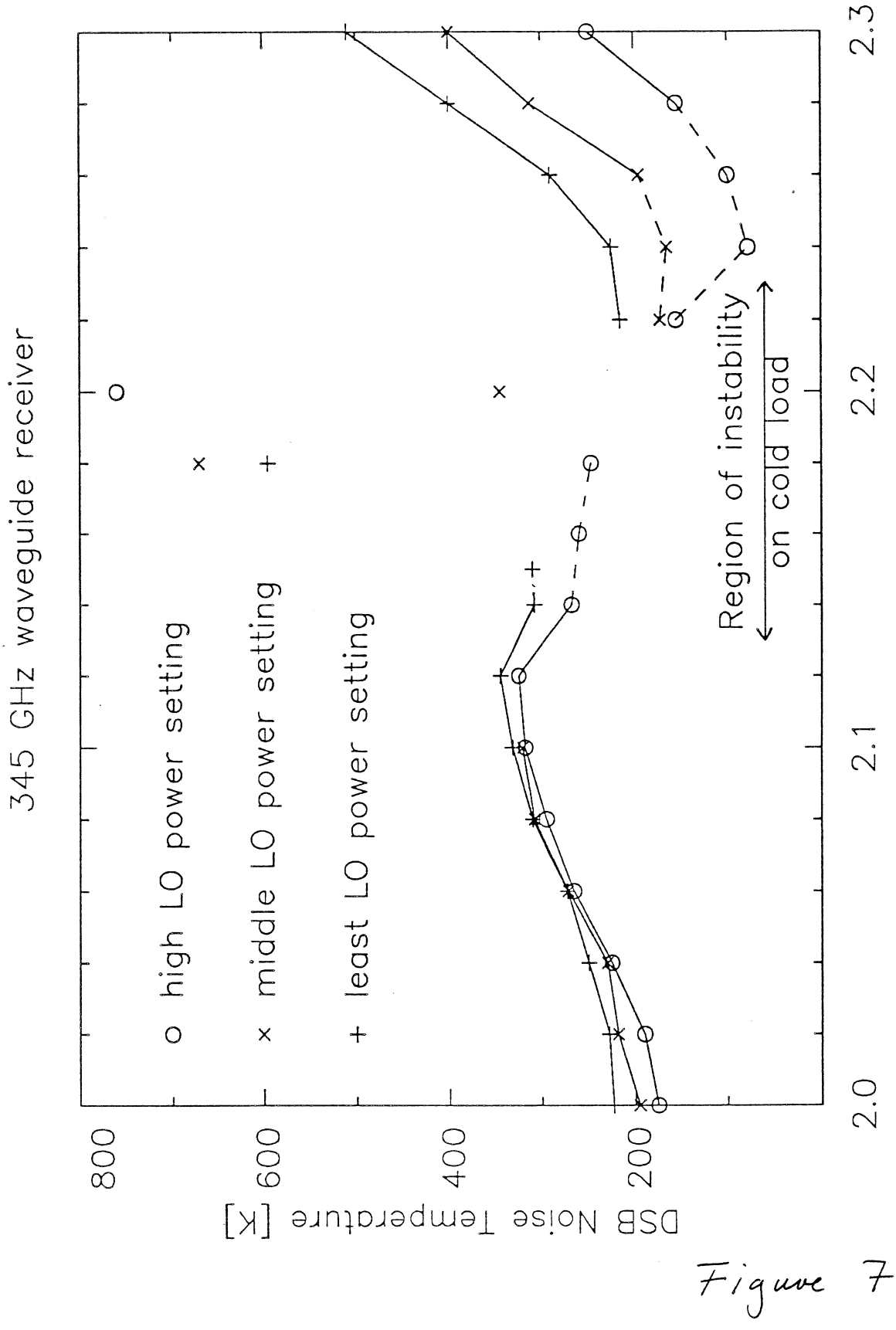
345 GHz waveguide receiver
o high LO power setting
x middle LO power setting
+ least LO power setting
Region of instability
on cold load
DSB Noise Temperature [K]
800
600
400
200
2.0
2.1
2.2
2.3
Bias Voltage [mV]

Figure 7

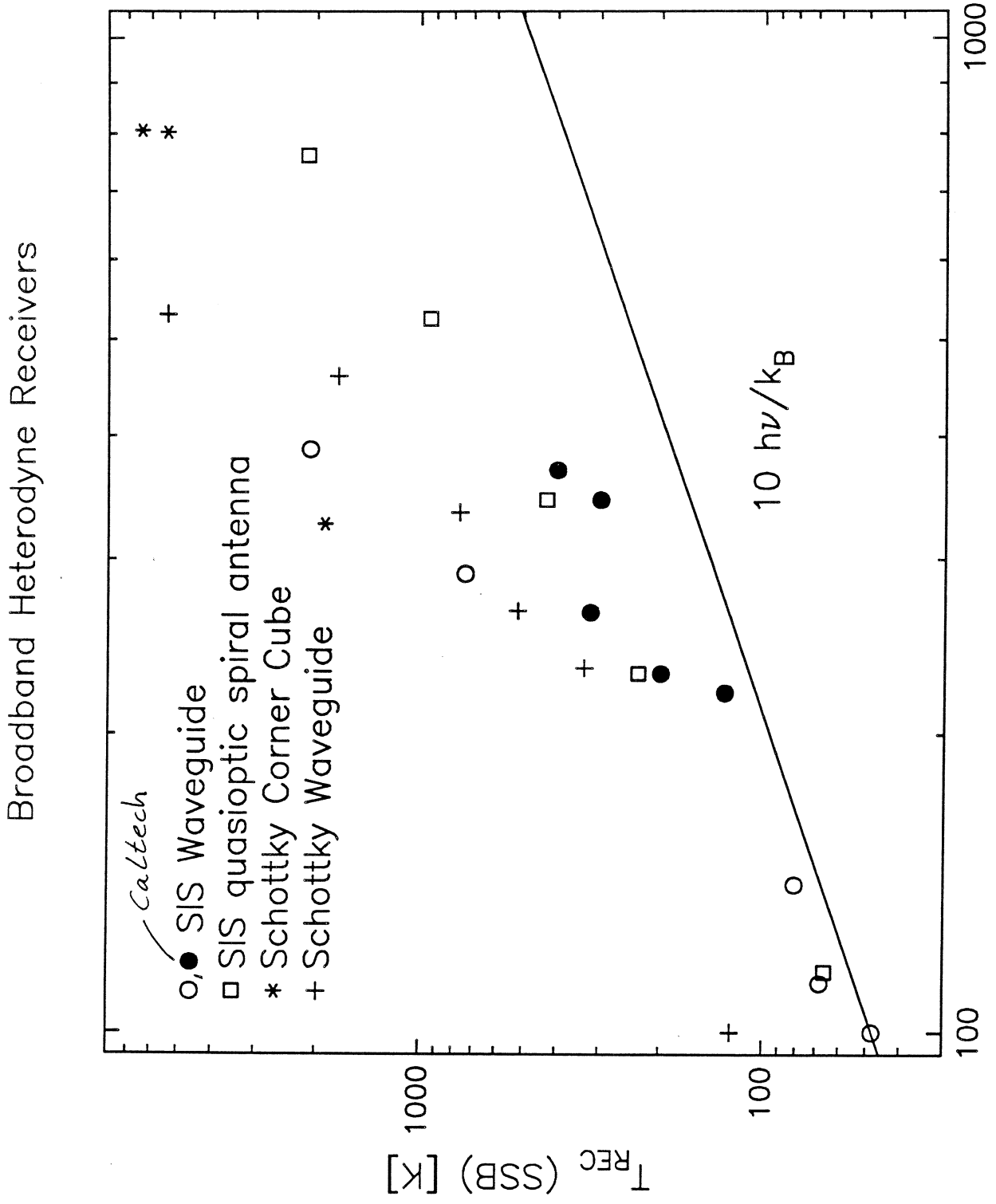
Broadband Heterodyne Receivers
Caltech
o, ● SIS Waveguide
□ SIS quasioptic spiral antenna
* Schottky Corner Cube
+ Schottky Waveguide
10 hν/k_B
T_REC (SSB) [K]
1000
100
100
1000
Frequency [GHz]

Figure 8

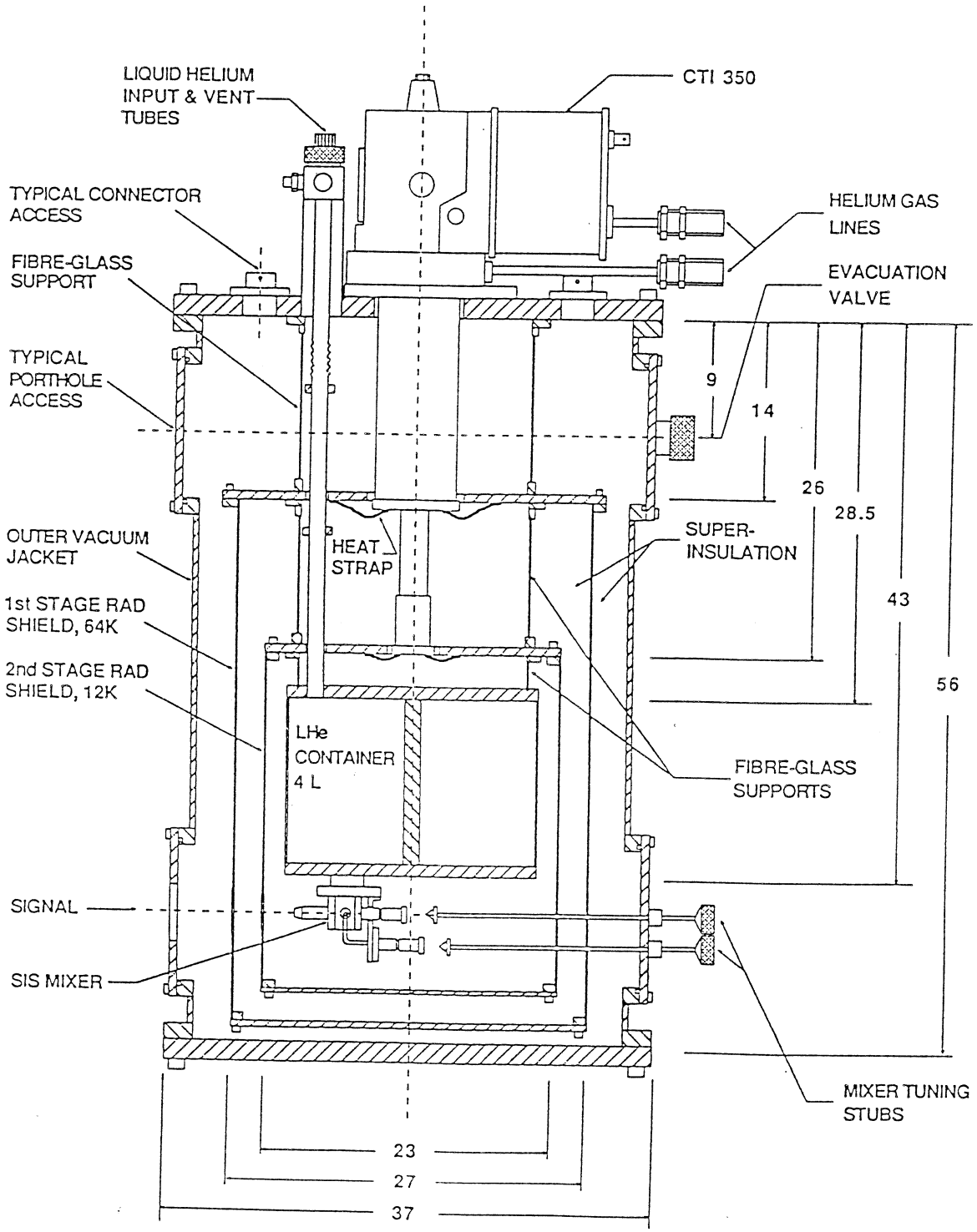
LIQUID HELIUM INPUT & VENT TUBES
CTI 350
TYPICAL CONNECTOR ACCESS
HELIUM GAS LINES
FIBRE-GLASS SUPPORT
EVACUATION VALVE
TYPICAL PORTHOLE ACCESS
9
14
26
28.5
43
56
OUTER VACUUM JACKET
HEAT STRAP
SUPER-INSULATION
1st STAGE RAD SHIELD, 64K
2nd STAGE RAD SHIELD, 12K
LHe CONTAINER 4 L
FIBRE-GLASS SUPPORTS
SIGNAL
SIS MIXER
MIXER TUNING STUBS
23
27
37

Figure 9

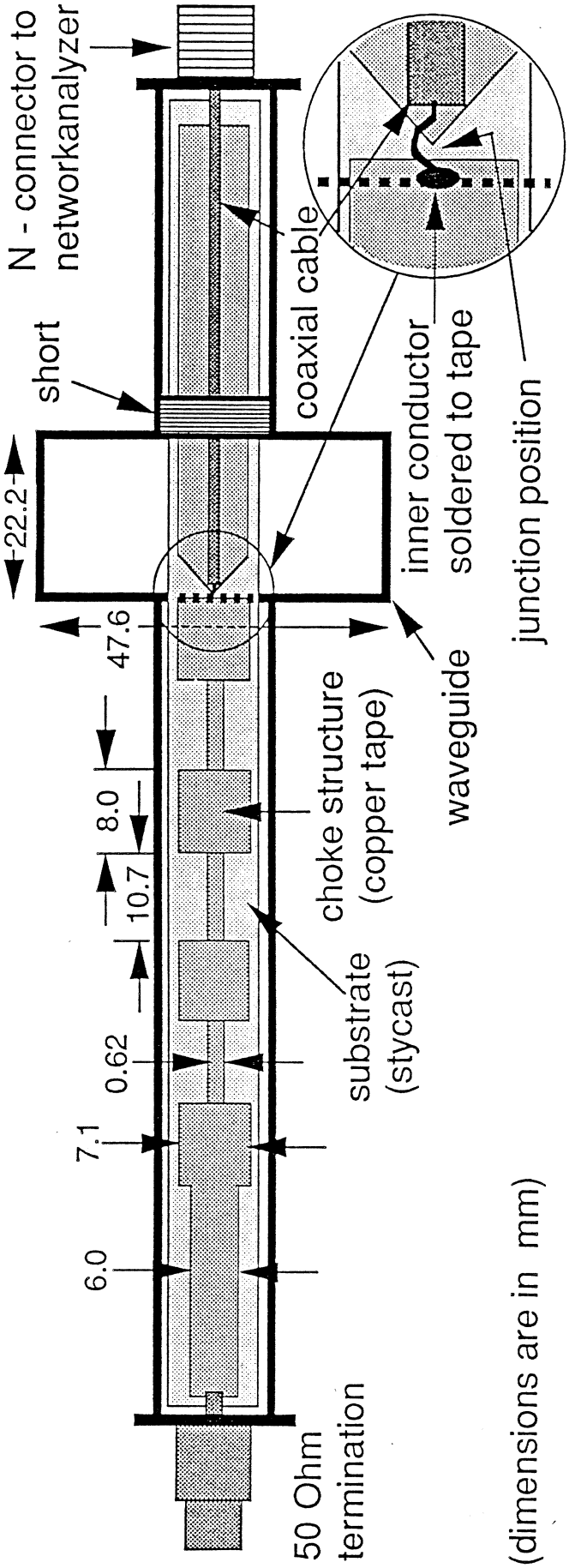
N - connector to networkanalyzer
short
coaxial cable
inner conductor soldered to tape
junction position
22.2
47.6
waveguide
choke structure (copper tape)
8.0
10.7
substrate (stycast)
0.62
7.1
6.0
50 Ohm termination
(dimensions are in mm)

Figure 10

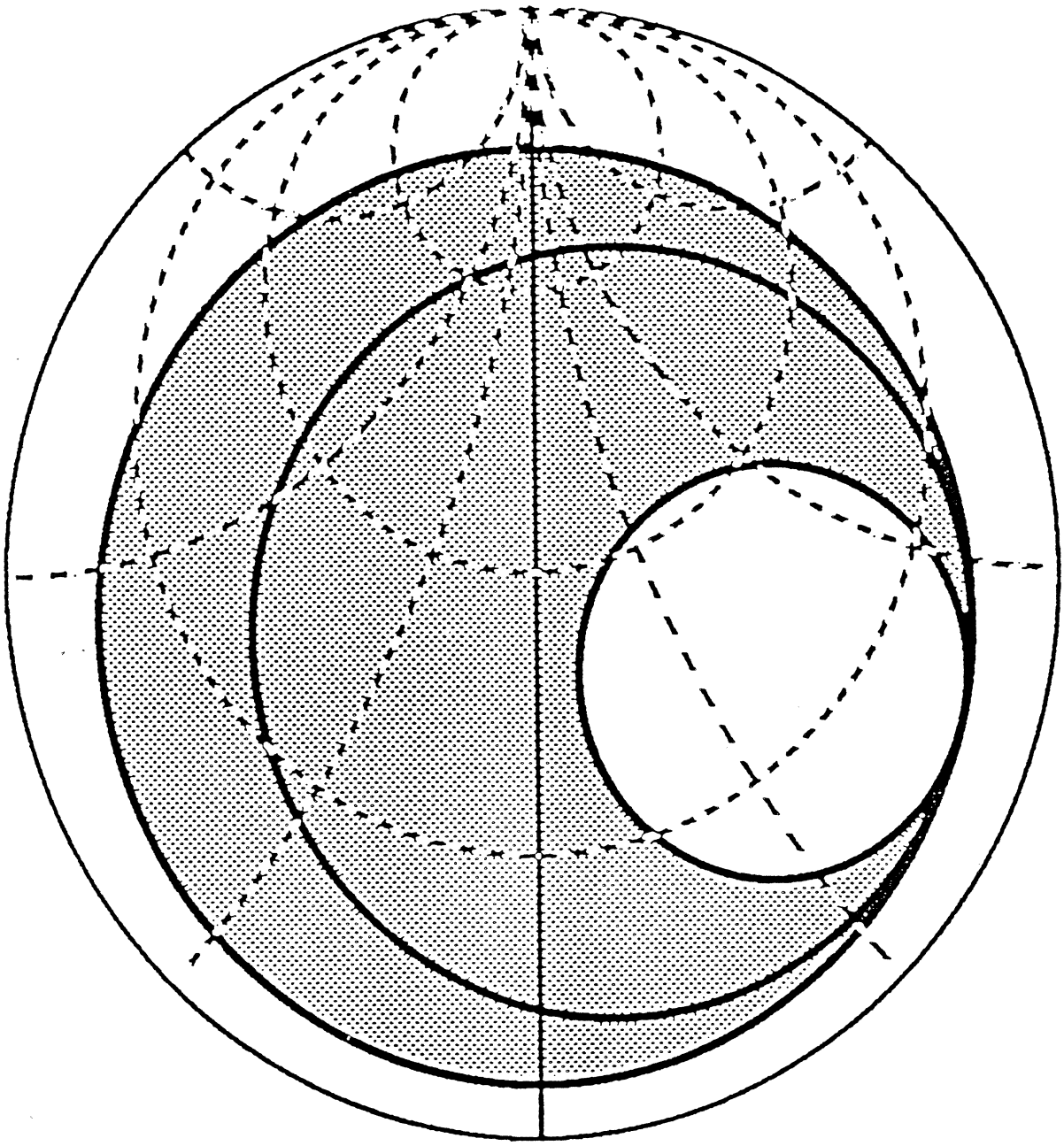

Smith chart normalized to 50Ω

Figure 11

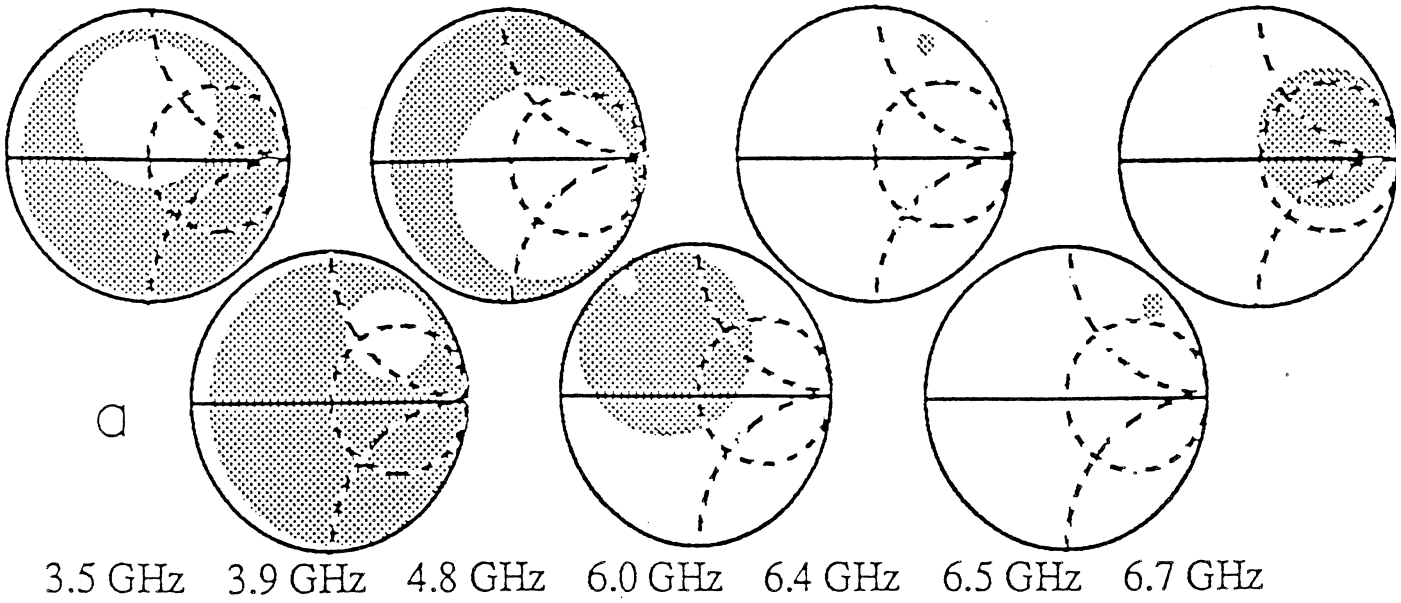
a
3.5 GHz
3.9 GHz
4.8 GHz
6.0 GHz
6.4 GHz
6.5 GHz
6.7 GHz

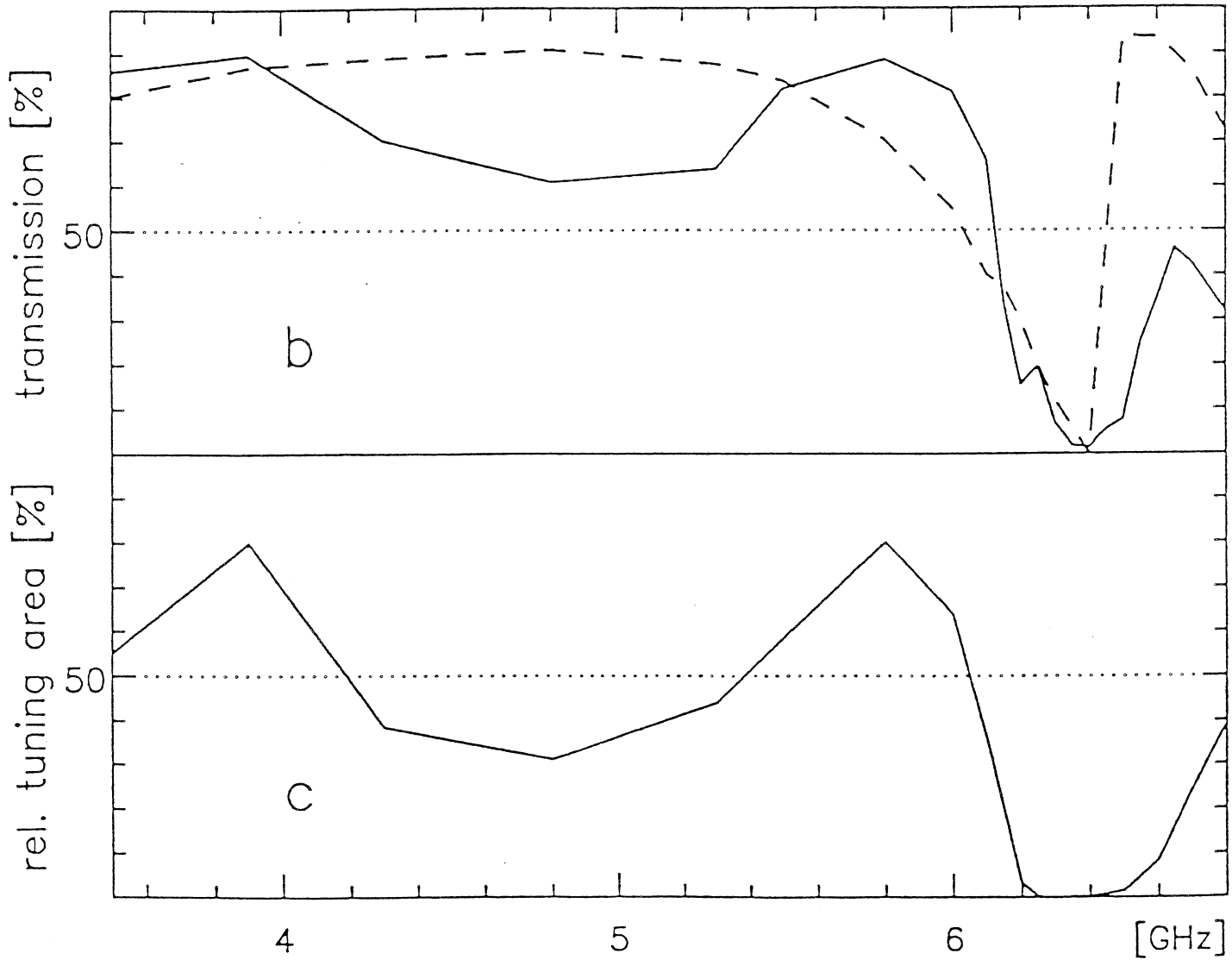
transmission [%]
50
b
rel. tuning area [%]
50
c
4
5
6
[GHz]

Figure 12

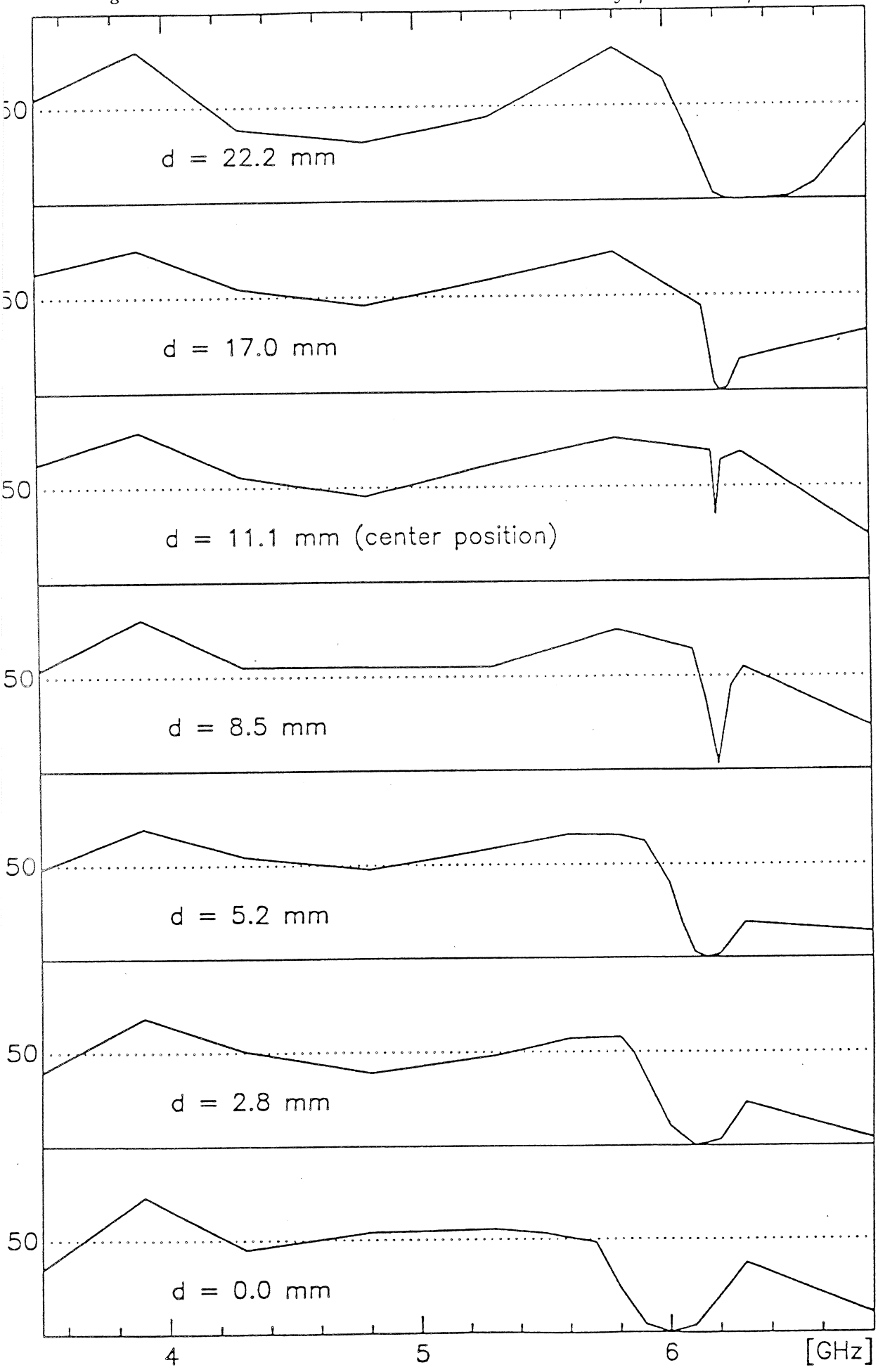
50
d = 22.2 mm
50
d = 17.0 mm
50
d = 11.1 mm (center position)
50
d = 8.5 mm
50
d = 5.2 mm
50
d = 2.8 mm
50
d = 0.0 mm
4
5
6
[GHz]

Figure 13

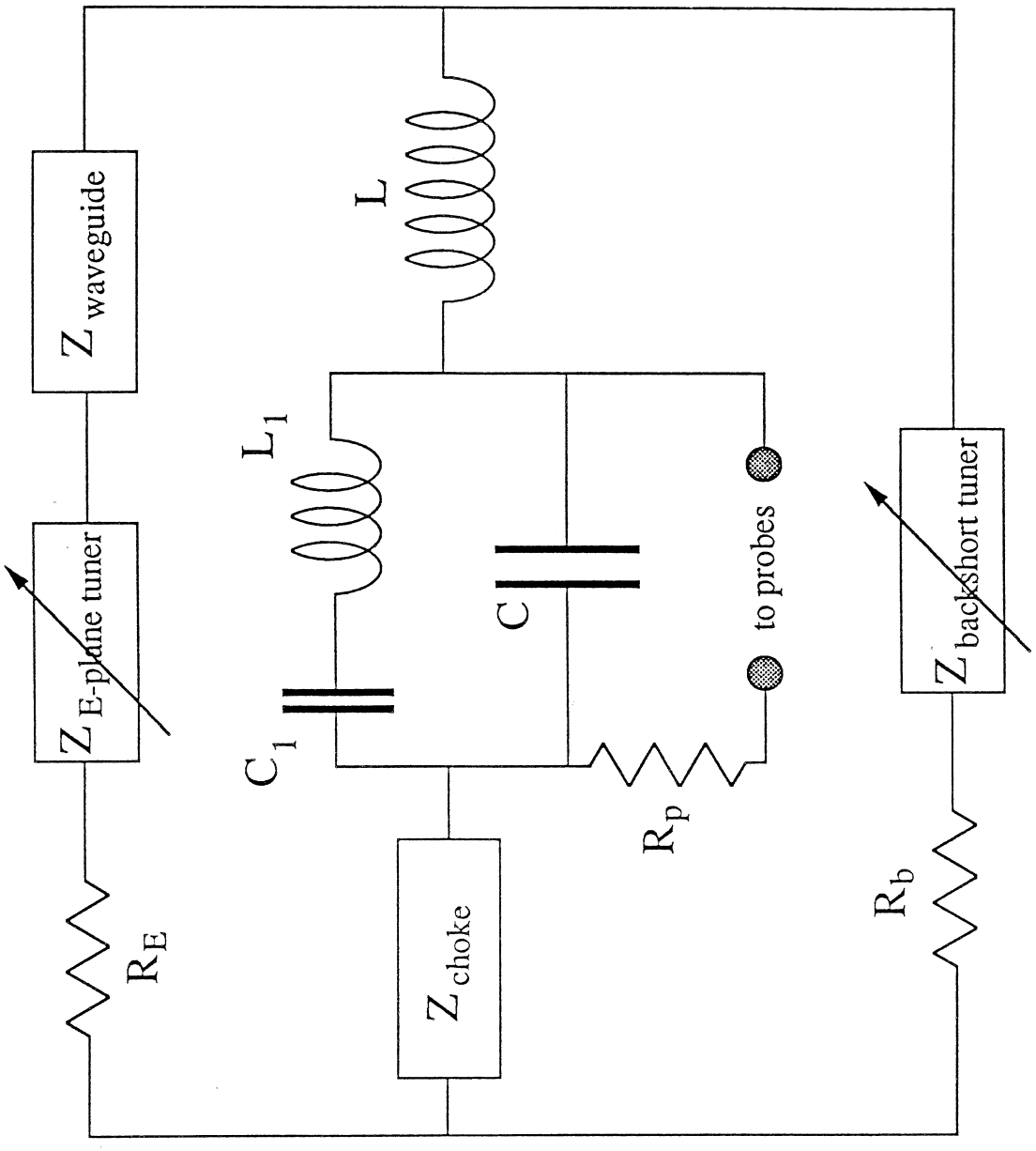
Z waveguide
Z E-plane tuner
R_E
L
L_1
C_1
C
to probes
R_p
Z choke
Z backshort tuner
R_b

Figure 14

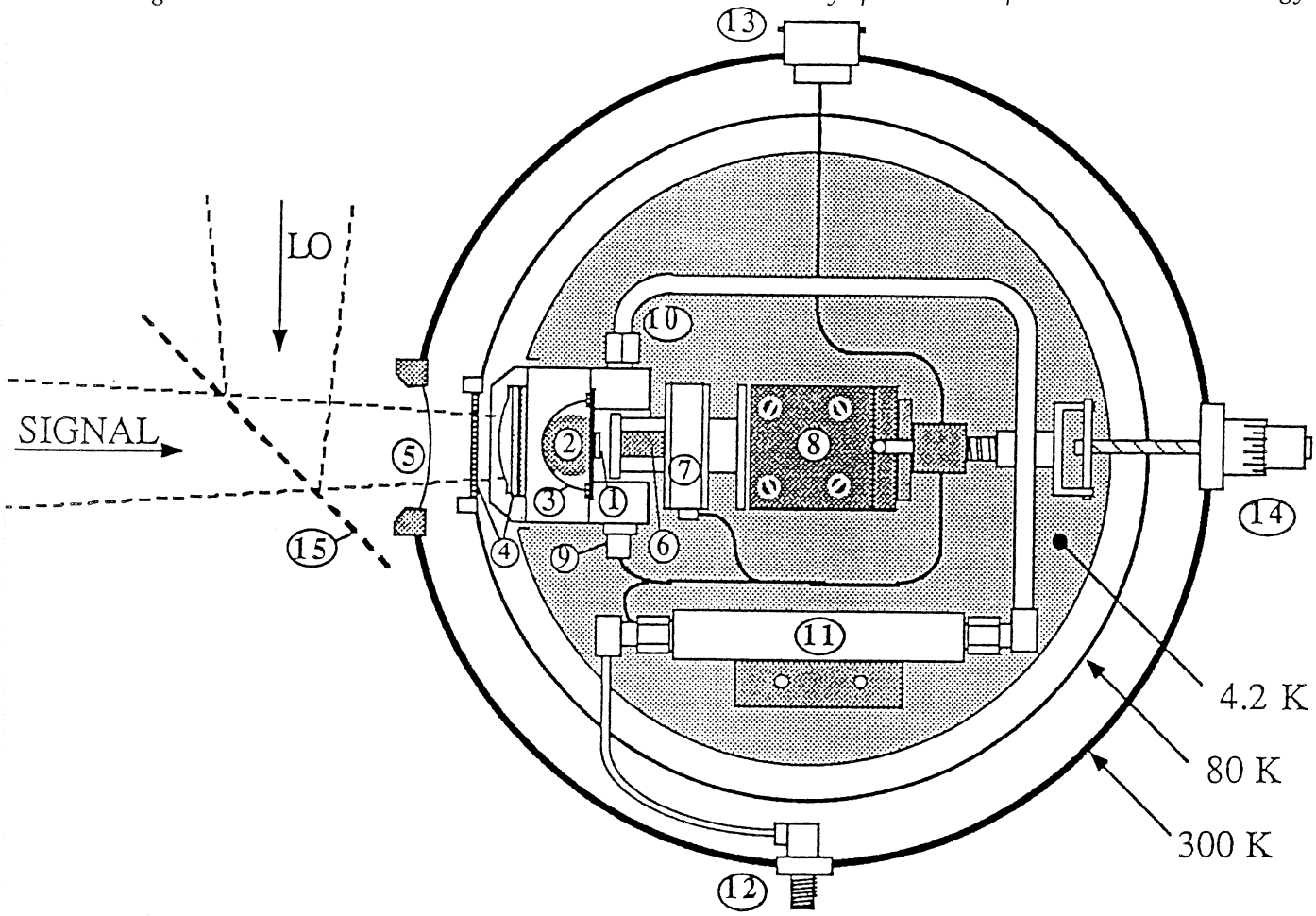

1 Spiral antenna with SIS junction
2 Hyperhemisphere
3 Anti reflection coating
4 IR filters and plastic lens
5 Mylar window
6 Conductive plane with Fe core
7 Coil for magnetic field
8 Translation stage
9 SIS junction DC-bias
10 Mixer IF output
11 IF preamplifier
12 IF output
13 Electronics connector
14 Conductive backplane drive
15 Beam splitter

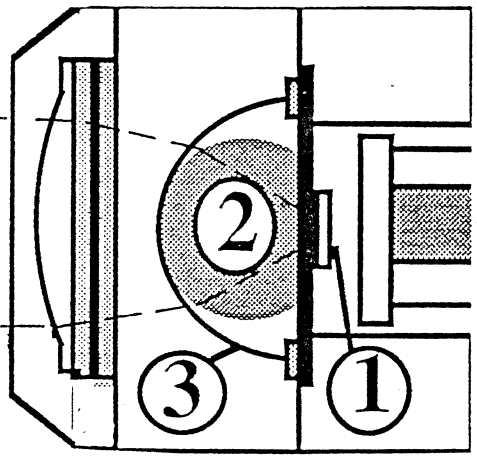

Mixer block

Figure 15

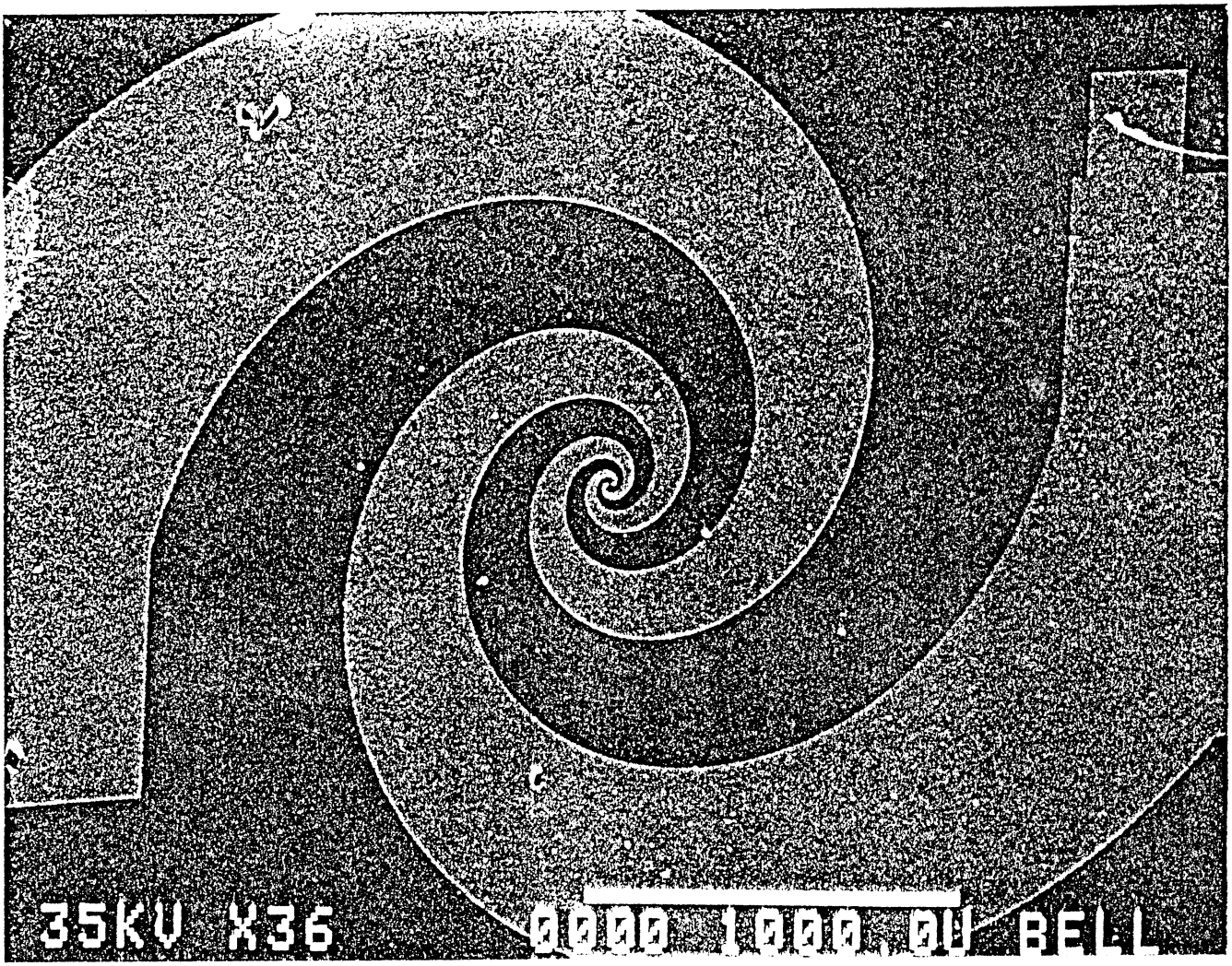

Figure 16

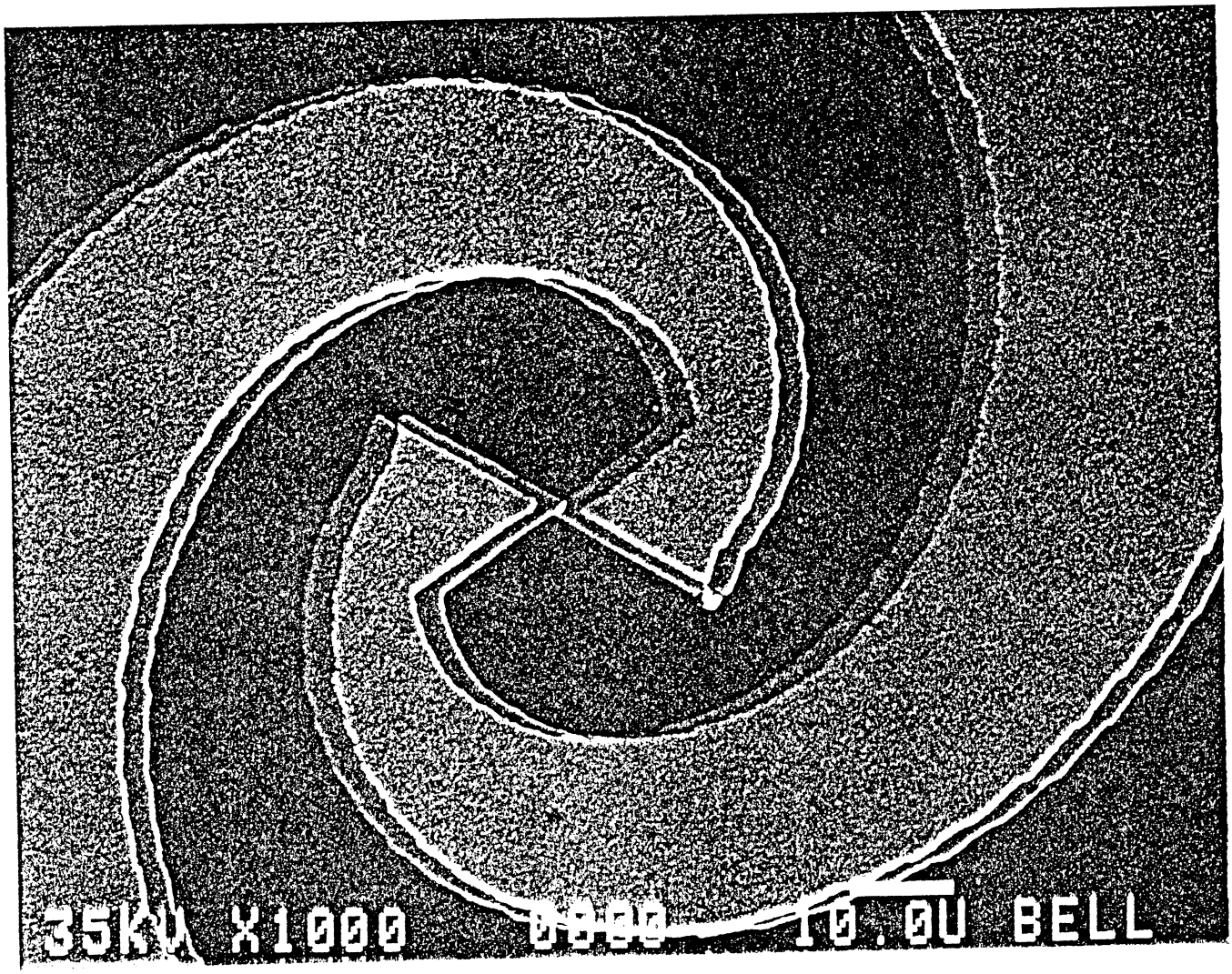

Figure 17